Proceedings of the 12th International Conference on Heat Transfer and Fluid Flow (HTFF 2025)

Paris, France - August, 2025 Paper No. HTFF 211 DOI: 10.11159/htff25.211

Physics Informed Neural Networks for Temperature Fields of Convective Heat Transfer

ChiIao Ma¹, QingLong Jin², Yan Su³

Department of Electromechanical Engineering, FST, University of Macau, Taipa, Macau mc45171@connect.um.edu.mo; yc47440@connect.um.edu.mo; yansu@um.edu.mo

Abstract – A physics informed neural network (PINN) improved from the artificial neural network (ANN) is applied for prediction of temperature fields for convective heat transfer in a two-dimensional channel. The inlet flow at a constant high temperature is cooled by the square channel walls at constant low temperature and is fully developed at the outlet. The entrance lengths for the temperature and velocity fields are varying. The PINN integrates physical information into the network structure for training, which makes implement of the physical constraints practical. In the present study, the physical constraints are presented by the residuals of the heat transfer equations. Both ANN and PINN can provide good prediction results for both temperature and heat transfer coefficient distributions. Compared to the ANN, the PINN with residuals of the heat transfer equations can obtain a higher accuracy in predicting temperature fields and converge at faster speeds.

Keywords: Artificial neural network; Convective heat transfer; Nusselt number; Physics informed neural network

1. Introduction

With the development of machine learning, Artificial Neural Network (ANN) has been widely used to solve various physical problems such as furnace mechanics, heat transfer, and mechanics. [1-3] However, NNs do not directly consider the physical equation as a data fitting method that does not allow strict physical consistency. Physical equation constraints are added to the loss function for physics informed neural network (PINN) [4,5] to ensure the solutions are not only data-driven but also conform to the physical laws of the problem being studied. Therefore, PINNs are able to immediately process complex and nonlinear problems that are difficult to solve with traditional numerical methods, especially partial differential equations (PDE) problems in high dimensions and complex geometries.

Many researchers have introduced PINN into natural convection problems. Wang et al. [6] applied PINN to flow and heat transfer problems in natural conventions and analyzed the influence of the number of training datasets to the prediction of natural convection velocity fields and temperature fields in PINN when the Reynolds number under 1000 is put into practice. It was found that for natural convection problems with complex geometries, more sample points are needed for PINN to achieve better prediction results for natural convection problems with complex geometries. A composed framework based on PINN and graph convolution network (GCN) is introduced by Peng et al. [7] and has exhibited excellent geometric adaptation and prediction capability. In comparison to purely data-driven ANN, this framework effectively reduced the error between the prediction results and actual values. The effect of variables such as the loss function, optimizer, network structure and activation function is analyzed on the accuracy and convergence of PINN by Hashemi et al. [8]. The results show that PINN is able to fit the temperature and velocity fields in natural convection better. However, in the condition of a higher Rayleigh number, the accuracy of the prediction is compromised by too few sample points.

In addition to natural convection problems, PINN has also been applied to other typical thermodynamic and fluid dynamic problems. Jalili et al. [9] demonstrated the energy transfer and flow properties during the growth of vapour bubbles in superheated liquids using PINN technologies. Three different fluids are used to conduct the testing. Through combining the results of the analytical solutions and CFD calculations, a stable simulation of the liquid-gas phase change process during fluid evaporation and capturing the effect of surface tension is offered by PINN. Jin et al.[10] have introduced PINN to problems such as cylindrical bypassing to analyze the influences of dynamic weights and fixed weights on improving the accuracy of PINN and the relationship between the loss of boundary conditions and the loss of residual error of the governing equation. A combination of thermal image technologies and PINN is applied by Cai et al. [11]. They proposed a new method based on PINNs to infer the full continuous three-dimensional (3D) velocity and pressure fields from snapshots of 3D

temperature fields obtained by thermal image technologies. By only relying on the temperature fields provided by thermal image technologies, the instantaneous velocity and pressure overlying the espresso are able to be simulated and the influence results of PINNs for unsteady velocity fields in the central plane were verified through independent example image velocity experiments.

Raissi et al. [12] established two different algorithm types for continuous time models and discrete time models by studying the data-driven equation solving and the identification of partial differential equations for data-driven by applying PINN. Moreover, Raissi et al. [13] investigated the problems of the free vibration of a cylinder due to the lift using PINN. The corresponding physical equations were derived based on the PINN inversions of unknown physical parameters such as Reynolds numbers and Peclet numbers. A PINN model that gets rid of the dependence on datasets was proposed by Li et al. [14]. In this PINN model, the original data loss function was replaced by the physical loss. Through iterative training, a three-dimensional temperature field was effectively predicted without labelled data. In comparison to the prediction results of this PINN model with the finite element calculation results, the maximum relative error was about 2%. Apart from this, the PINN model can quickly improve the calculation speed while maintaining the accuracy through introducing transfer learning methods.

In the present study, a PINN improved from the artificial neural network (ANN) is applied for prediction of temperature fields for convective heat transfer. Prediction accuracy and convergence speed of PINN will be compared with those of ANN.

2. Problem Definition and Governing Equations

The sketch of the physical model and boundary conditions are plotted in Fig. 1. As shown in Fig. 1, the constant high temperature flow runs into the square channel with a constant high temperature T_{high} and velocity u_{in} . Boundary walls of the channel are fixed at low temperature T_{low} . With a length scale of the channel height L=H, velocity scale u_{in} , temperature scale $\Delta T = T_{\text{high}} - T_{\text{low}}$, the dimensionless numerical model is shown in Fig. 1. The corresponding dimensionless governing equations for conservation of momentum and thermal energy are shown as

(1)

where Re is the Reynolds number, Pe is the Peclet number defined as Pe = RePr.

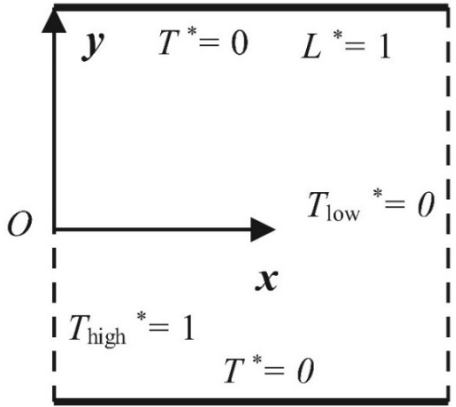


Fig.1: The sketch of the convective diffusion model with boundary conditions

3. Prediction with Physical Loss

The structure of an ANN is plotted in Fig. 2 (a). It can be seen that the model consists of a multi-layer network structure including an input layer, a hidden layer and an output layer. The neural network calculates the objective function through forward propagation and back propagation is used to transmit the error that affects the weight matrix and bias vector. The forward propagation follows the following linear and non-linear variations to fit the objective function

(2)

where σ is the activation function and defined as tanh function. Back propagation is the core algorithm for training neural networks and is also the most critical step. It is mainly used to optimize the weights and biases of the network through gradient descent to minimize the loss function. The loss function measures the difference between the actual value and the predicted value through the network. MSE Loss L_{data} is selected as

$$(3)$$

where o_i is the prediction value of the neural network, y_i is the ground truth (GT) value, i represents the number of features of the prediction value.

The improved structure of a PINN is shown in Fig. 2 (b). The PINN is extended from the basis of traditional artificial neural network. The extra layers of gradients are automatically calculated during the feed forward step. Then, the gradients obtained are applied to calculate the residuals of the governing equations, which is applied as the physical loss as

The total loss function of PINN consists of two parts: the data loss and the physical loss. Hence, the total loss is composed by two items as

$$L = L_{\text{data}} + L_{phy} \tag{5}$$

Then, the loss function influences the weight matrix and bias vector through back propagation. By adding the physical residual loss to the total loss function and influencing the weight matrix through back propagation, the neural network is restricted by physics information and fitting an objective function that satisfies the partial differential equations with higher accuracy.

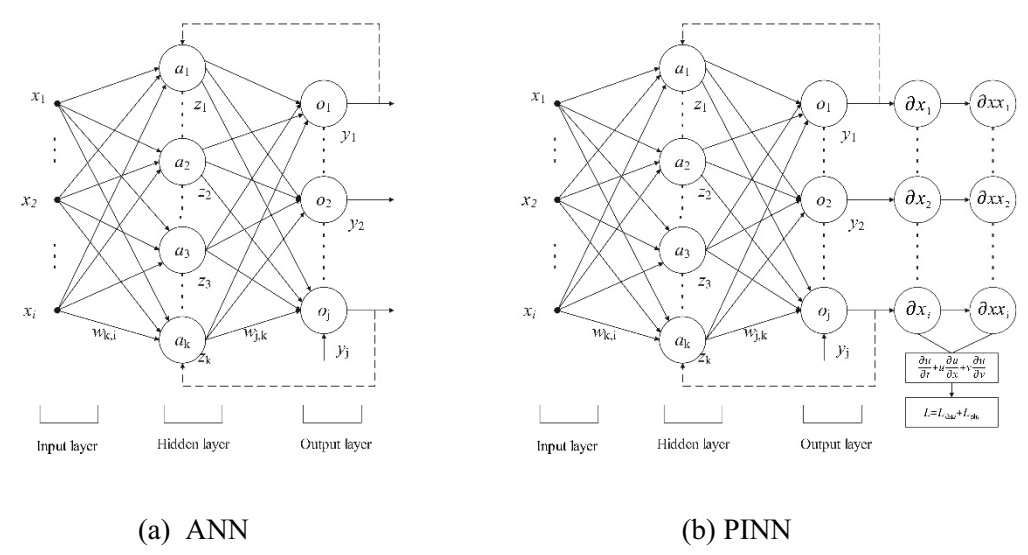


Fig. 2: A diagram for comparison of the two structures of the ANN and PINN.

4. Results and Discussion

4.1. Loss function and accuracy

The data loss functions with the training set epoch of the two types of prediction models are plotted in Fig. 3. As illustrated in Fig. 3, whether it is ANN or PINN, the data loss based on the training and validation sets gradually decreases with the increases of epoch and the convergence of two models both reaches a stable level. It needs to be clarified that for the training set, there is no significant difference between the ANN model and the PINN model at the initial stage. While, the training set for PINN at the end results in a slightly higher value than the ANN. However, it is noticeable that the loss function of PINN is obviously lower than ANN using the validation set. This result shows that the performance of PINN is improved effectively by adding partial differential equations as residuals. In comparison with ANN calculation results, PINN effectively reduces the data loss and improves the model performance as a model that contains physical information. A further analysis and comparison of the accuracy of the two models are shown in Fig. 4. As shown in the figure, whether it is the training or validation sets, the accuracy calculated by the PINN model is higher than the prediction result of the ANN model. Compared to the ANN, the accuracy of PINN is about 3% higher, and the loss function converged at a speed of 4.2% faster.

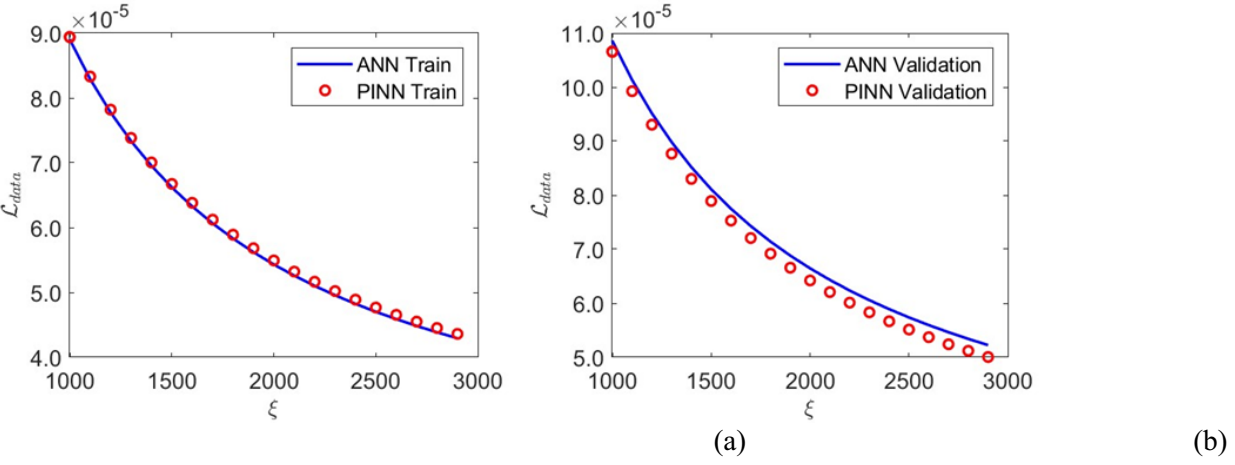


Fig. 3: Comparison of the loss function curves of ANN, PINN models

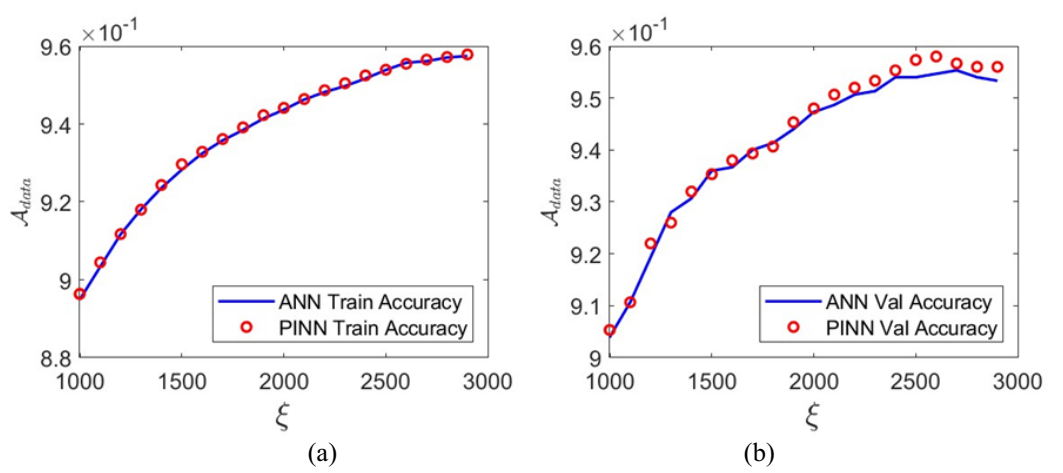


Fig. 4: Comparison of the accuracy curves of ANN, PINN models

4.2. Velocity fields

The distribution of horizontal velocity component u is shown in Fig. 5. A constant velocity inlet condition is imposed on the left side of this velocity field and fluid flows from left to right where it is a free outflow. As simulation time progresses, the internal velocity field gradually develops into steady state fully developed flow profiles with the velocity for top and bottom boundaries being zero and the velocity in the middle is relatively higher, which forms a steady flow structure of an acceleration of velocity from left to right. Due to the fact that the initial inlet velocity is constant, the fluid is affected by the wall friction after entering the channel and the velocity of the cross section is generally transmitted from uniform distribution to typical parabolic distribution. It is also found out that the entrance length is about 0.4L. In the central and downstream regions (x>0.4L) in the channel, the distribution of contour lines is converging to parallel and the cross-section of velocity is steady. The flow has evolved into a fully developed laminar structure with typical characteristics of maximum velocity at the middle and a rapid decrease in velocity at the boundaries. The whole velocity field maintains symmetry along the x-axis and presents a typical dynamic behavior of a two-dimensional stable flow field.

The distribution of the vertical direction velocity field v is displayed in Fig. 6. As shown in Fig. 6, the entire velocity field v contains four zones. The velocity v is gradually converting from negative to positive along the y-axis. This is because the inlet velocity is distributed at a constant speed and without a vertical gradient, resulting in a rapid shear near the top and bottom walls after entering the fluid and the backflow formed near the upper wall surface by obstruction which is a typical boundary layer separation effect. Similar to the upper wall surface, the velocity near the wall surface is zero because the lower wall surface is no-slip. The amplitude of velocity v fluctuations is diminished and progressively approaches zero in this region. This situation indicates that fluid returns to the main horizontal transportation state and the flow is dominated along the x-axis by the u velocity. Meanwhile, the gradients of v decrease when approaching the outlet. According to Figs. 6 (b) and (c), the prediction results based on the ANN and PINN models are essentially similar to the GT results.

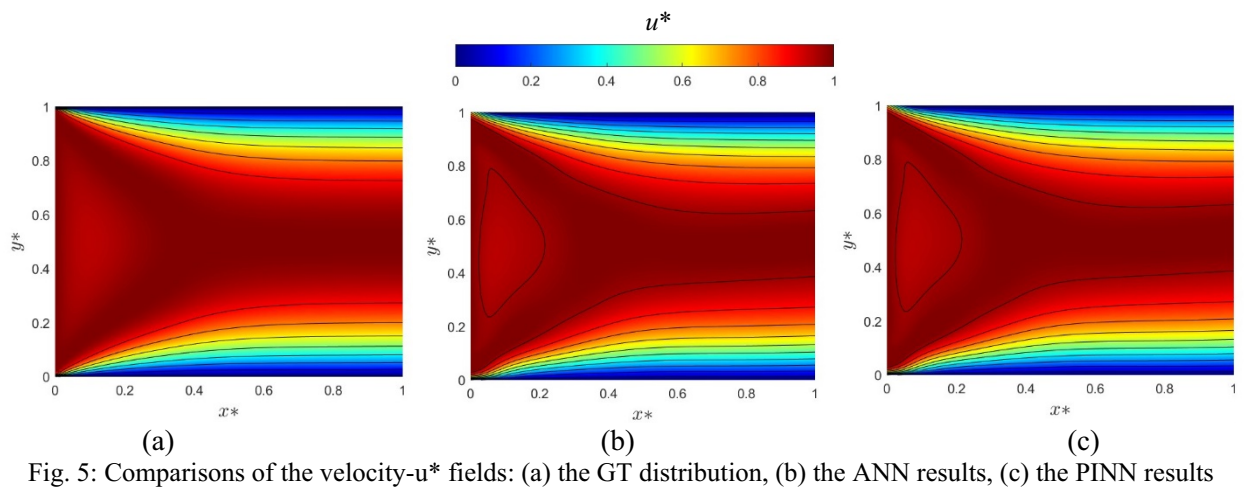
4.3. Temperature fields

The temperature fields are shown in Fig. 7. As shown in Fig. 7 (a), the temperature is highest at the position x=0 which is the boundary of the red heat source. The temperature is gradually reducing along the x direction. It can be clearly seen that the heat is mainly transported along the horizontal flow direction and continuously diffuses vertically towards the upper and lower boundaries during the process which forms a typical convection-diffusion coupled temperature field structure. The isotherms show a more obvious temperature gradient and thermal boundary layer effect in the figure because the lines are dense and curved near the boundary. In parallel, the central area remains at a higher temperature. The distribution of temperature in the right outlet area is moderately tend toward gentle which reflects the natural dissipation process of heat flow in the channel. This indicates that the heat flow is mainly driven by horizontal transportation and maintains a strong vertical diffusion. With comparison of the u velocity field in Fig. 5, the entrance length of the temperature field is much larger than the entrance length of the flow field. From Fig. 7(b) and 7(c), both ANN and PINN predicted the temperature field well.

The Nusselt numbers predicted by ANN and PINN are compared with the GT results in Fig. 8. Where Nu_x is the Nusselt number along the x direction, and Nu_y is the Nusselt number along the y direction. The scaled values according to the reference Nu_{ref} are defined as

$$Nu^* = Nu / Nu_{\text{ref}} \tag{5}$$

The block dots are $Nu_y^*(x)$ at the bottom boundary along the channel length in x^* direction, reflecting the characteristics of gradual weakening of the temperature gradient at the wall as the flow is developed. The red diamonds represent the $Nu_x^*(y)$ at the left wall along the y^* direction, exhibiting a symmetrical distribution in which the temperature gradient is maximum near the wall and minimum at the central axis. Two curves are highly consistent with the temperature field temperature which revealing the variation rule of local heat transfer intensity with spatial location under convection-diffusion coupling.



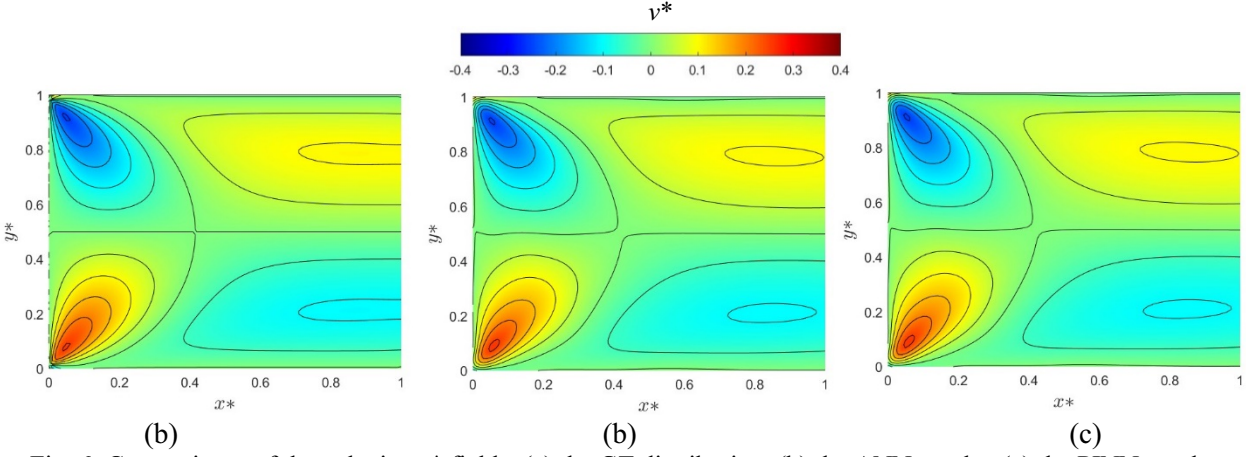


Fig. 6: Comparisons of the velocity-v* fields: (a) the GT distribution, (b) the ANN results, (c) the PINN results

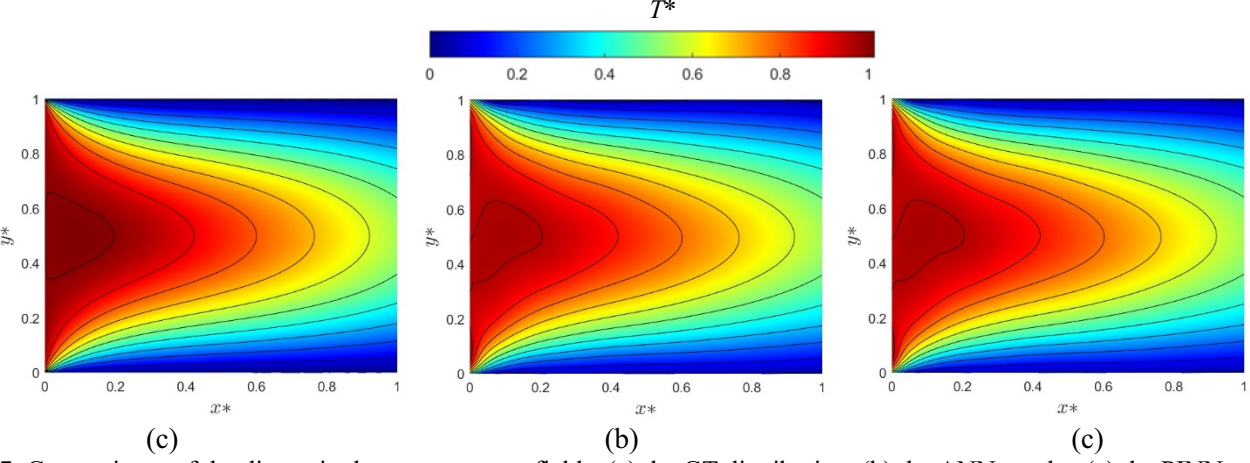


Fig. 7: Comparisons of the dimensionless temperature fields: (a) the GT distribution, (b) the ANN results, (c) the PINN results

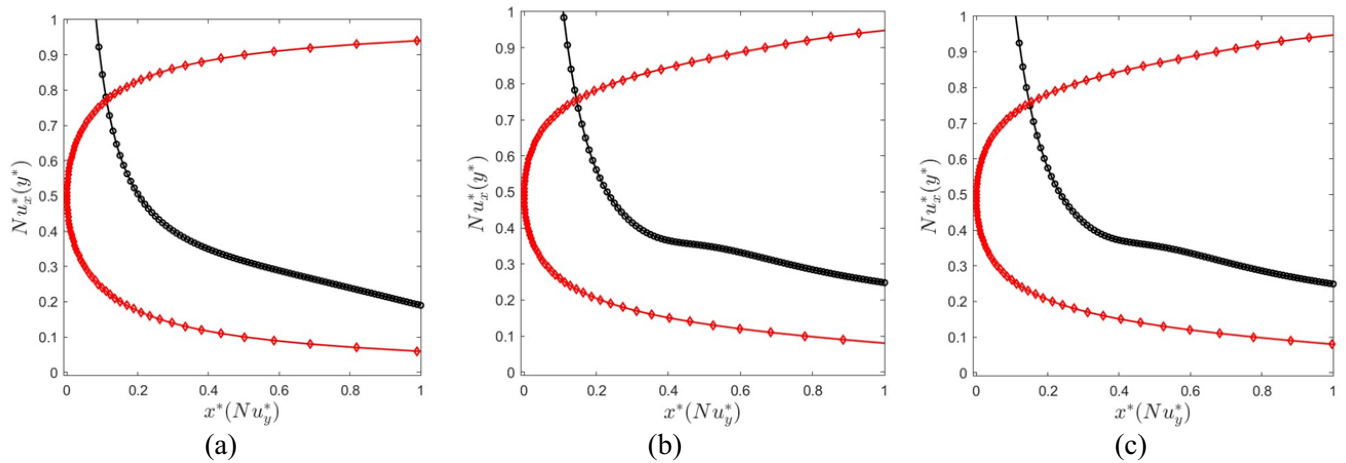


Fig.8: Comparisons of the Nusslet number: (a) the GT distribution, (b) the ANN results, (c) the PINN results

4. Conclusion

The temperature and velocity fields of convective heat transfer in a square channel are predicted by both ANN and PINN. The results show that PINN model performance better compared to conventional ANN with extra physics information represented by the residuals of the governing equations. Compared to the ANN, the accuracy of PINN is about 3% higher, and the loss function converged at a speed of 4.2% faster.

Acknowledgements

This study was supported by the projects with the sponsorship of the Science and Technology Development Fund, Macao S.A.R (FDCT) with the project number FDCT/0142/2022/A. Also thanks the High Performance Computing Cluster of Information and Communication Technology Office of the University of Macau.

References

- [1]. J. Kim, C. Lee, Prediction of turbulent heat transfer using convolutional neural networks, Journal of Fluid Mechanics, vol. 882, A18, 2020.
- [2]. K. Jambunathan, S. L. Hartle, S. Ashforth-Frost, E. J. T. Webb, Evaluating convective heat transfer coefficients using neural networks, International Journal of Heat and Mass Transfer, vol. 39, no. 11, pp. 2329–2332, 1996.
- [3]. Y. Liu, N. Dinh, Y. Sato, K. Shirvan, Data-driven modeling for boiling heat transfer: Using deep neural networks and high-fidelity simulation results, Applied Thermal Engineering, vol. 144, pp. 305–320, 2018.
- [4]. S. Cuomo, V. S. D. Cola, F. Giampaolo, G. Rozza, M. Raissi, F. Piccialli, Scientific machine learning through physics—informed neural networks: Where we are and what's next, Journal of Scientific Computing, vol. 92, no. 3, 88, 2022.
- [5]. H. Bui, W. Jing, Applications of physics-informed neural networks in power systems A review, IEEE Transactions on Power Systems, vol. 38, no. 1, pp. 572–588, 2023.
- [6]. T. Wang, Z. Huang, Z. Sun, Y. Lu, Reconstruction of natural convection within an enclosure using deep neural network, International Journal of Heat and Mass Transfer, vol. 164, 120626, 2021.
- [7]. J. Peng, N. Aubry, Y. Li, M. Mei, Z.H. Chen, W.T. Wu, Physics-informed graph convolutional neural network for modeling geometry-adaptive steady-state natural convection, International Journal of Heat and Mass Transfer, vol. 216, 124593, 2023.
- [8]. Z. Hashemi, M. Gholampour, M. C. Wu, J. Lee, A physics-informed neural networks modeling with coupled fluid flow and heat transfer Revisit of natural convection in cavity, International Communications in Heat and Mass Transfer, vol. 157, 107827, 2024.

- [9]. D. Jalili, M. Jadidi, A. Keshmiri, P. W. Chan, Transfer learning through physics-informed neural networks for bubble growth in superheated liquid domains, International Journal of Heat and Mass Transfer, vol. 232, 125940, 2024.
- [10]. X. Jin, S. Cai, H. Li, G.E. Karniadakis, NSFnets (Navier-Stokes flow nets): Physics-informed neural networks for the incompressible Navier-Stokes equations, Journal of Computational Physics, vol. 426, 109951, 2021.
- [11]. S. Cai, Z. Wang, F. Fuest, Y.J. Jeon, C. Gray, G.E. Karniadakis, Flow over an espresso cup: inferring 3-D velocity and pressure fields from tomographic background oriented Schlieren via physics-informed neural networks, Journal of Fluid Mechanics, vol. 915, A102, 2021.
- [12]. M. Raissi, P. Perdikaris, G. E. Karniadakis, Physics-informed neural networks: A deep learning framework for solving forward and inverse problems involving nonlinear partial differential equations, Journal of Computational Physics, vol. 378, pp. 686–707, 2019.
- [13]. M. Raissi, Z. Wang, M.S. Triantafyllou, G. E. Karniadakis, Deep learning of vortex-induced vibrations, Journal of Fluid Mechanics, vol. 861, pp. 119–137, 2019.
- [14].S. Li, G. Wang, Y. Di, L. Wang, H. Wang, Q. Zhou, A physics-informed neural network framework to predict 3D temperature field without labeled data in process of laser metal deposition, Engineering Applications of Artificial Intelligence, vol. 120, 105908, 2023.